

Provide a one page executive summary, with necessary supporting information in an appendix. The situation is outlined below.

Situation:

You graduate with your BS in ME or ABE in December 2008 and go to work for a large soy oil processing and biodiesel mixing company. Although the company doesn't manufacture engines, it is highly interested in the effect that biodiesel will have on engine performance, specifically emissions. Many sources state that emissions, specifically oxides of nitrogen (NO_x) from engines running biodiesel are much higher than their fossil fueled counterparts. As a research and marketing effort, your company wants to better understand why this is happening and provide engineering support and consultation (at a cost) to engine manufacturers to help eliminate this disparity. The company views this as a key effort to increase the demand for one of its key products.

To that end, you have been hired as one of the first engineers on this project. Your manager has been brought in from a major engine manufacturer. He has experience in combustion and combustion modeling in their efforts to reach Tier 3 and Tier 4 emissions.

You spent a month learning about combustion in several training trips. Next you created a proposal to develop internal knowledge in your team. The first step in this multi-million dollar project is to do some basic instrumentation of an engine on a dynamometer, as outlined in Chapter 3 of *Off-Road Vehicle Engineering Principles* (Goering et. al., 2003). You choose the John Deere 4045 Tier I engine to look at how mechanical injection systems deal with regular vs. biodiesel and spend the next month setting everything up and getting good data. You ran your first run with ordinary #2 Diesel. Although you have no results with any biodiesel mixes, upper management would like a short report (Executive Summary) on your preliminary findings and what this could possibly mean when you start working with biodiesel. Your manager knows you are very busy, but this will be distributed to his manager (an engineer, but not knowledgeable in engines/fuels) and others above him or her (non-engineers), so it needs to be top notch.

You've shown your manager some charts of the pressure and heat release curves (derived from laboratory tests). He wants to see your analysis of why those curves look the way they do. He's also heard that biodiesel advances injection and ignition. You find an article on ASABE's website that discusses this (Monyem et al., 2001).

The people that will be seeing this don't want to see raw data, they want to see figures with logical analysis, comparisons, contrasts, etc. These people determine your salary and, perhaps more importantly, how much money you get to play with next year.

Don't just answer the questions presented here. Develop your own questions. Don't just connect the dots, prove that you understand enough to develop your own picture. The objective of this lab is to force you to prioritize the importance of the information you present and target this information for the audience (Lead Engineer and non-technical upper level management). In addition in industry you will almost always be give incomplete information and instructions to complete the task. The expectation is that you have the training, initiative and ability to complete the task.

ENGINE HEAT RELEASE VIA SPREAD SHEET

C. E. Goering

ABSTRACT. Calculation of rates of heat release from engine fuels provides a useful diagnostic tool. As one example, the technique was useful in discovering that retarding injection timing will reduce the proportion of premixed combustion and thereby reduce NO_x emissions from a diesel engine. The technique for calculating heat release rates was proposed more than 30 years ago. Initially a cumbersome technique, it has been simplified over the years. In the present work, the author presents equations which allow calculation of heat release rates within a spread sheet.

Keywords. Fuels, Heat release, Diesel engine, Spread sheet.

Calculation of rates of heat release from engine fuels provides a useful diagnostic tool. For example, combustion of methyl esters of vegetable oils typically produce NO_x emissions higher than those from petroleum-based diesel fuel. Scholl (1985) found that NO_x emissions could be reduced by retarding the start of injection to reduce the proportion of premixed burning; it has been found that NO_x emissions are produced in premixed burning but not in diffusion burning.

Kreiger and Borman (1966) were the first to propose a method for inferring the rate of heat release from fuels. By rapid measurement of combustion chamber pressures at frequent intervals, it is possible to infer the work done on the piston, the increase in internal energy of the trapped mixture, and the heat transfer through the combustion chamber walls, and to total these quantities to calculate the heat released during each increment of crankshaft rotation.

Pressures must be measured at high speed. Experience has shown that measurements should be made at least once per 0.25° of crankshaft rotation to adequately capture the variation in heat release during a combustion cycle. For an engine running at 2,400 rpm, 57,600 pressure measurements per second are required. When Faletti et al. (1984) used the Kreiger and Borman method to determine heat release rates from hybrid fuels, it was necessary to record the pressures on a high-speed, FM tape recorder, play the tape into a digitizer at lower speed, and then enter the digitized pressure data into a main frame computer. Later, PCs became fast enough that Sorenson et al. (1986) were able to capture the pressure directly using a PC and

then use special software in analyzing the pressure data to determine rates of energy release. The data were then transferred to a spread sheet for plotting.

The objective of the present study was to develop a spread sheet capable of calculating heat release rates directly. It would be necessary to import the pressure data and corresponding crankshaft angles into the spread sheet, then the spread sheet would do all calculations necessary to determine heat release rates.

THEORY

Although combustion in a CI, DI (compression-ignition, direct-injection) engine is quite heterogeneous, the contents of the combustion chamber are assumed to be homogeneous in the heat release calculations described by Sorenson et al. (1986). This type of heat release model is referred to in the literature as a zero-dimensional model. Some investigators (e.g., Hanson, 1989) have developed more complex, quasi-dimensional models, but these are only slightly more accurate than the zero-dimensional model. SI primary units, kg-m-s, and secondary units derived from them are used in the equations which follow. More convenient units are entered into the spread sheet (e.g., cylinder bore in cm rather than in m) and the spread sheet converts them as needed for use in calculations. Sorenson et al. presented the following equation for heat release:

$$\frac{dQ}{d\theta} = \frac{V \frac{dP}{d\theta} + \gamma P \frac{dV}{d\theta}}{\gamma - 1} - \frac{dQ_w}{d\theta} \quad (1)$$

where

$dQ/d\theta$ = rate of heat release ($J/^\circ$)

V = gas volume (m^3)

θ = crank angle ($^\circ$)

P = cylinder pressure (Pa)

γ = ratio of specific heats

$dQ_w/d\theta$ = rate of heat transfer from the wall ($J/^\circ$)

The first two columns in the spread sheet contain the crank angles and the corresponding measured cylinder pressures.

Article was submitted for publication in July 1997; reviewed and approved for publication by the Power & Machinery Div. of ASAE in July 1998.

This manuscript was prepared expressly for consideration for publication in the *Transactions of the ASAE*. Mention of commercial products is for information only and does not constitute an endorsement by the University of Illinois or express a preference over similar products not mentioned.

The author is **Carroll E. Goering, ASAE Member Engineer**, Professor, Agricultural Engineering, 360 AESB, University of Illinois, 1304 W. Pennsylvania Ave., Urbana, IL 61801; tel: (217) 333-2969; fax: (217) 244-0323; e-mail: ceg@age2.age.uiuc.edu.

In a four-cycle engine, crank angles are typically given with zero at the HDC (head dead center) between the intake and exhaust strokes. However, the important heat release events occur between SOI (start of injection, typically about 340°) and EVO (exhaust valve opening, typically about 500°). Also, spread sheet trigonometric functions require their arguments in radians. Thus, the following transformation is included in the spread sheet:

$$\theta_{\text{rad}} = \frac{\pi(\theta - 360 + \text{phase})}{180} \quad (2)$$

where

θ_{rad} = argument of trigonometric functions (radians)
 phase = phase shift angle (°)

Typically, an encoder is used to measure crankshaft angles. Precise alignment between the encoder HDC and the piston HDC is required for accurate heat release determinations. If the two HDCs are misaligned by “phase” degrees, equation 2 corrects for the misalignment.

The piston displacement, needed in calculating the gas volume, is given by:

$$\frac{S}{R} = \left[1 - \cos(\theta_{\text{rad}}) \right] + \frac{L}{R} \left\{ 1 - \sqrt{1 - \left[\frac{\sin(\theta_{\text{rad}})}{\frac{L}{R}} \right]^2} \right\} \quad (3)$$

where

S = piston displacement from HDC (m)
 R = radius to crank pin (m)
 L = connecting rod length (m)
 Then the gas volume can be calculated:

$$V = V_{\text{cl}} + S A_p \quad (4)$$

where

A_p = top area of piston (m²) = $\pi(\text{bore})^2/4$
 bore = cylinder bore (m)
 V_{cl} = clearance volume (m³) = $D_1/(r - 1)$
 r = compression ratio
 D_1 = cylinder displacement (m³) = A_p (stroke)
 stroke = piston stroke (m)

Also, the combustion chamber wall area, needed for heat transfer calculations, is approximately:

$$A_{\text{wall}} = 2A_p + \pi(\text{bore}) S \quad (5)$$

Equation 5 ignores the area associated with the piston cup, but the approximation has little effect on the heat release results.

The heat release equation (eq. 1) requires the calculation of $dP/d\theta$. It can be shown that the slope at the j th point of the curve defined by n sequential points is:

$$\frac{dP_j}{d\theta} = \frac{n \sum (P_i \theta_i) - \sum (P_i) \sum (\theta_i)}{n \sum (\theta_i^2) - (\sum \theta_i)^2} \quad (6)$$

where n is an odd number and each summation is from $[j - (n - 1)/2]$ to $[j + (n - 1)/2]$. When a shaft encoder is used to trigger pressure measurements, the points are equally spaced along the θ axis at spacing $\Delta\theta$. The choice of n is a compromise; a larger n helps combat noise in the pressure data, but may also obscure real changes in the heat release curve. When $\Delta\theta = 0.25^\circ$, choice of $n = 13$ fits equation 6 over 3° of the pressure trace and is a suitable compromise. For $n = 13$, when the pressure data are equally spaced at intervals $\Delta\theta$, it can be shown that:

$$\frac{dP_j}{d\theta} = \frac{(1P_{k+1} + 2P_{k+2} + \dots + 13P_{k+13}) - 7 \sum (P_i)}{182 \Delta\theta} \quad (7)$$

where $k = [j - (n - 1)/2 - 1] = [j - 7]$ when $n = 13$. If $\Delta\theta = 0.25^\circ$ is used in equation 7, then $dP_j/d\theta$ will be given in units of Pa/°. If heat release per 0.25° is desired, then use $\Delta\theta = 1$ in equation 7 and $dP_j/d\theta$ will be given in units of Pa/0.25°.

Noise in the pressure signal is very disruptive to heat release calculations. Before doing any other calculations involving the pressure, a smoothing technique is usually applied to the pressure curve. The following is a suitable smoothing technique:

$$P_{j+1} = P_j + \frac{dP_j}{d\theta} \Delta\theta \quad (8)$$

In applying equations 7 and 8, it is necessary to include at least $[(n - 1)/2]$ data points prior to SOI, so that the smoothed pressures are accurate beginning at SOI. Smoothing is accomplished first, by incorporating equation 7 with $\Delta\theta = 1$ into equation 8 with $\Delta\theta = 0.25^\circ$. Then equation 7 (with $\Delta\theta = 1$) is applied to the smoothed data to calculate the pressure derivatives.

Calculation of $dV/d\theta$ is easily accomplished, as follows:

$$\frac{dV_j}{d\theta} = V_j - V_{j-1} \quad (9)$$

If the data points are spaced at $\Delta\theta = 0.25^\circ$, then the units of $dV/d\theta$ will be m³/0.25°.

The value of γ varies with temperature and the gas temperature is also needed in calculating heat transfer to the wall. The ideal gas law is used to calculate the spatially averaged temperature in the combustion chamber, i.e.:

$$T_j = \frac{P_j V_j}{M R_g} \quad (10)$$

where

T_j = bulk gas temperature at point j (°K)
 R_g = idea gas constant = $8.314/29 = 0.287$
 M = mass of charge, $g = (1 + AF) m_f$
 AF = air/fuel ratio of engine
 m_f = mass of fuel injected into each engine cycle (g)

The value of γ varies with temperature and the gas temperature is also needed in calculating heat transfer to

the wall. It can be shown that the value of γ can be calculated from the following equation:

$$\gamma = \left(1 - \frac{R_g}{C_p}\right)^{-1} \quad (11)$$

According to Crowell (1989), the value of C_p/R_g can be calculated from:

$$\frac{C_p}{R_g} = A_0 + A_1 T_j + A_2 T_j^2 + A_3 T_j^3 + A_4 T_j^4 \quad (12)$$

where

$$\begin{aligned} C_p &= \text{specific heat of gas at constant pressure (J/kg}\cdot\text{K)} \\ A_0 &= 3.04473 \\ A_1 &= 1.33805E-3 \\ A_2 &= -4.88256E-7 \\ A_3 &= 8.55475E-11 \\ A_4 &= -5.70132E-15 \end{aligned}$$

The final term in equation 1 is $dQ_w/d\theta$, the term to account for heat transfer through the wall. It is calculated from:

$$\frac{dQ_w}{d\theta} = \frac{h A_{\text{wall}} (T_w - T_j)}{24 N} \quad (13)$$

where

$$\begin{aligned} dQ_w/d\theta &= \text{heat transfer, J/0.25}^\circ \\ T_w &= \text{Effective wall temperature (}^\circ\text{K)} \\ h &= \text{convective heat transfer coefficient} \\ &\quad \text{(J/s}\cdot\text{m}^2\cdot\text{K)} \\ N &= \text{engine speed (rpm)} \end{aligned}$$

The heat transfer calculations are not very sensitive to the wall temperature, T_w ; a wall temperature of $T_w = 485^\circ\text{K}$ has been found to give satisfactory results. Eichelberg (1939) developed the following equation for convective heat transfer:

$$h = 0.00767 S_p^{0.333} (P_j T_j)^{0.5} \quad (14)$$

where

$$\begin{aligned} S_p &= \text{mean piston speed, m/s} = 2 R \omega / \pi = 2 (\text{stroke}) \\ &\quad N/60 \\ \omega &= \text{crankshaft speed (rad/s)} \end{aligned}$$

PRESSURE MEASUREMENTS

The typical method for measuring combustion chamber pressures is to install a sleeve through the engine head and install a pressure transducer in the sleeve. To avoid pressure signal oscillations, it is necessary that the sensing face of the transducer be nearly flush with the top of the combustion chamber. A water-cooled transducer can survive the high temperatures; also, the face of the transducer is coated with RTV rubber cement to further protect the transducer against radiative heat transfer. A model 8QP-500 ca, water-cooled, piezoelectric pressure transducer from the AVL Company is suitably fast and robust to accomplish the pressure measurements. AVL will also supply a reservoir and pump system to circulate

distilled water through the transducer. A charge amplifier must be used to condition the signal from the piezoelectric transducer; A Kister model 504 charge amplifier is suitable. Typically, the transducer-charge amplifier system is calibrated by exposing the transducer to known pressures.

A shaft encoder is used to measure crankshaft angle. A BEI model 25G-1440-ABZ-7404-LED-ED15 optical shaft encoder has been found to give satisfactory results. This two-channel encoder produces an HDC pulse on one channel and a pulse each 0.25° of crankshaft rotation on the other channel. Typically, when pressure measurements are desired, the HDC signal is used to start pressure measurements at each 0.25° of crankshaft rotation. For good results, 20 to 100 consecutive cycles must be recorded and then averaged together, point by point, to obtain an averaged cycle for heat release analysis. Averaging more cycles is more accurate, but requires more computer memory for data storage.

As previously mentioned, correct phasing between the HDC of the encoder and that of the piston is very important. Correct phasing is most easily accomplished if it is possible to motor the engine, i.e., to cause it to run at normal speed without fuel. Then, the logarithm of the pressure is plotted versus the logarithm of the volume. By adjusting the phase angle in equation 2 before calculating the logarithm of the volume, the shape of the log P – log V plot can be changed; the proper shape is when the compression and expansion processes superimpose on each other as straight lines.

AN APPLICATION

A Lister-Petter two-cylinder, water-cooled, DI diesel engine was used to obtain pressure data for heat release analysis. A AVL 8QP-500 ca pressure transducer was installed to measure cylinder pressures, while a BEI model 25G-11140-ABZ-7404-LED-ED15 shaft encoder was used to measure crankshaft position. A Kister model 504 charge amplifier was used to condition the pressure signal. The engine cylinder bore was 86 mm, the stroke was 80 mm, and the compression ratio was 18. While operating at 2,200 rpm, with each cylinder producing 20 N.m of torque, each cylinder consumed 16 g/s of air and 0.4 g/s of No. 2 diesel fuel. A General Electric model TLC-7.5 electric dynamometer was used to provide engine load and, to enable encoder phasing, to motor the engine at 2,200 rev/min. A Log P – Log V plot from the motoring test was plotted to obtain the phase offset angle, which was entered into equation 2. Data for 20 consecutive cycles were taken while the engine was under load, then the cycles were averaged to obtain a cycle for heat release analysis. The pressure data and corresponding crank angles were entered into the first two columns of the heat release spread sheet. Adjoining columns were used to calculate quantities given by equations 1 through 14 above, with equation 1 being the last column in the spread sheet. The first 35 lines of the 800-line spread sheet are shown in figure 1. The observed bore, stroke, connecting rod length, compression ratio, engine speed, air and fuel consumption per cylinder were entered into the spreadsheet as shown in figure 1. Also entered were the estimated wall temperature and any needed phase shift and zero shift in the pressure trace. The heat release results are relatively insensitive to

Engine: Lister-Petter

CI Vol= 27.34 cm³ *N= 2200 rev/min
 *Bore= 8.6 cm Sp= 5.867 m/s
 *Stroke= 8 cm *Mairdot= 16 g/s hconst= 0.00767 J/s/m²/oK
 *C. R. L.= 12 cm *Mf1dot= 0.4 g/s
 L/R= 3
 Pist. A. = 58.09 cm² M cyl1= 0.000458 kg
 *rc= 18

 *TempW= 485 Deg. K
 *Phase= 0.75 Deg.
 *Pshftdn= 0 kPa

Crank angle Degrees	Measured Pressure kPa	Smoothed Pressure kPa	Crank angle Radians	Cyl Vol cm ³	Del V cm ³ /de/4	Global Temp 1 Deg. K	Gamma	Wall Area cm ²	h 1 J/(m ² k)	dQw/dTHE J/deg/4	dP/dThe kPa/Deg/4	Heat Rel J/Deg/4
310.00	603	603	-0.8596	130.61		600	1.372	165.0	263.0	-0.00941		
310.25	602	602	-0.8552	129.67	-0.938	594	1.372	164.5	261.6	-0.00891		
310.50	611	611	-0.8508	128.73	-0.935	599	1.372	164.1	264.6	-0.00936		
310.75	605	605	-0.8465	127.80	-0.933	589	1.373	163.7	261.0	-0.00838		-2.0685
311.00	617	617	-0.8421	126.87	-0.930	596	1.372	163.2	265.2	-0.00909		-2.1065
311.25	628	628	-0.8378	125.94	-0.927	602	1.371	162.8	269.0	-0.00971		-2.1404
311.50	630	628	-0.8334	125.01	-0.924	598	1.372	162.4	268.4	-0.00931	33.06	8.9897
311.75	628	630	-0.8290	124.09	-0.921	595	1.372	161.9	267.4	-0.00904	39.44	11.0265
312.00	649	628	-0.8247	123.17	-0.918	589	1.372	161.5	270.4	-0.0086	43.65	12.3252
312.25	985	649	-0.8203	122.25	-0.915	604	1.363	161.1	337.4	-0.01226	46.51	13.4520
312.50	991	985	-0.8159	121.34	-0.912	910	1.340	160.6	415.3	-0.05367	47.16	13.3251
312.75	1006	991	-0.8116	120.43	-0.909	909	1.340	160.2	418.3	-0.05376	46.30	12.9015
313.00	1020	1007	-0.8072	119.52	-0.906	916	1.339	159.8	422.9	-0.05514	43.45	11.7621
313.25	1026	1020	-0.8029	118.62	-0.903	921	1.339	159.4	425.2	-0.05603	38.66	9.9484
313.50	1045	1026	-0.7985	117.72	-0.900	919	1.338	159.0	428.6	-0.05603	31.72	7.4397
313.75	1057	1045	-0.7941	116.82	-0.897	929	1.337	158.5	433.5	-0.0578	22.72	4.2072
314.00	1072	1057	-0.7898	115.92	-0.894	933	1.337	158.1	437.5	-0.05866	12.00	0.4392
314.25	1075	1073	-0.7854	115.03	-0.891	939	1.336	157.7	439.5	-0.05964	11.85	0.3156

Figure 1—Spread sheet for engine heat release.

the wall temperature and pressure zero shift. The results are highly dependent on the phase angle; the procedure for determining the correct phase angle was described earlier.

RESULTS

Figure 2 shows the heat release diagram from the Lister-Petter engine. SOI was at 348°. The dip in energy release after 348° reflects the energy required to evaporate the injected fuel. Ignition occurred at by 353.5°, as indicated by positive heat release following the evaporation dip. Thus, the ignition delay was 5.5°. During the ignition delay, the injected fuel must evaporate and mix with air; all

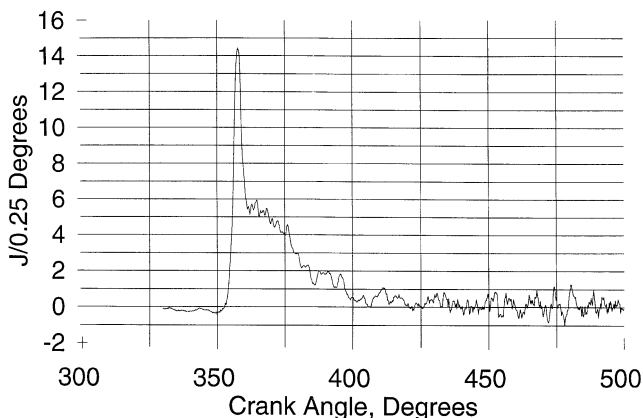


Figure 2—Heat release diagram from spread sheet.

of the mixture so prepared during the delay period burns quite suddenly when ignition occurs; the sharp spike in figure 2 is thus the premixed portion of the heat release diagram. While premixed burning is occurring, fuel vapor from the fuel-rich spray plumes and air from further out in the chamber begin to diffuse toward each other to continue the combustion. Thus, when premixed burning is completed, the heat release continues at a slower rate in what is called the diffusion burning mode. The spread sheet showed the premixed burning ending at approximately 363°, i.e., the duration of premixed burning was approximately 10°. As figure 2 shows, all burning was completed at approximately 420°; thus, the diffusion burning occurred at a much lower rate but much longer duration than the premixed burning.

DISCUSSION

The relative proportion of premixed burning could be increased and the diffusion proportion decreased by reducing the cetane rating of the fuel, reducing the load on the engine, or advancing the injection timing; the converse is also true and other factors also affect the heat release diagram. Premixed burning is efficient, but also produces NO_x emissions, engine knock and mechanical stress on the engine. Diffusion burning is quieter and less stressful on the engine, but also produces CO, HC, and smoke emissions and is less efficient. Thus, the balance between premixed and diffusion burning necessarily involves compromise. However, the availability of a technique for

plotting heat release diagrams allows that compromise to be made by the design engineer.

SUMMARY AND CONCLUSIONS

Calculation of rates of heat release from engine fuels provides a useful diagnostic tool. A technique for such calculations was suggested over 30 years ago; the procedure has become easier to use in the interim. The objective of the present work was to develop a means for calculating rates of heat release within a spread sheet. That objective was accomplished.

REFERENCES

- Crowell, T. J. 1989. Evaluation of enhanced ethanol with fumigation as a diesel fuel replacement. Unpub. M.S. thesis. Urbana, Ill.: University of Illinois.
- Eichelberg, G. 1939. Some new investigations on old combustion engine problems. *Engineering* 148: 463-464, 547-560.
- Faletti, J. J., S. C. Sorenson, and C. E. Goering. 1984. Energy release rates from hybrid fuels. *Transactions of the ASAE* 27(2): 322-325.
- Hanson, A. C. 1989. A diagnostic quasi-dimensional model of heat transfer and combustion in compression-ignition engines. Unpub. Ph.D. thesis. Pietermaritzburg, South Africa: Dept. of Agricultural Engineering, University of Natal.
- Kreiger, R. B., and G. L. Borman. 1966. The computation of apparent heat release for internal combustion engines. ASME Paper No. 66-WA/DPG4. New York, N.Y.: ASME.
- Scholl, K. W. 1985. Combustion performance and emissions of soybean methyl ester fuel in a DI diesel engine. Unpub. M.S. thesis. Urbana, Ill.: University of Illinois.
- Sorenson, S., T. K. Hayes, and L. D. Savage. 1986. Cylinder pressure data acquisition and heat release analysis on a personal computer. SAE Paper No. 860029. Warrendale, Pa.: SAE.

THE EFFECT OF TIMING AND OXIDATION ON EMISSIONS FROM BIODIESEL-FUELED ENGINES

A. Monyem, J. H. Van Gerpen, M. Canakci

ABSTRACT. *The alkyl monoesters of fatty acids derived from vegetable oils or animal fats, known as biodiesel, are attracting considerable interest as an alternative fuel for diesel engines. Biodiesel-fueled engines produce less carbon monoxide, unburned hydrocarbons, and particulate emissions than diesel-fueled engines. However, biodiesel has different chemical and physical properties than diesel fuel, including a larger bulk modulus and a higher cetane number. Some of these properties can be affected by oxidation of the fuel during storage. These changes can affect the timing of the combustion process and potentially cause increases in emissions of oxides of nitrogen.*

The objective of this study was to evaluate the effect of injection and combustion timing on biodiesel combustion and exhaust emissions. A John Deere diesel engine was fueled with two different biodiesel fuels, one of which had been deliberately oxidized, and with their 20% blends with No. 2 diesel fuel. The engine was operated at three different timings and two loads at a single engine speed of 1400 rpm.

The engine performance of the biodiesel was similar to that of No. 2 diesel fuel with nearly the same thermal efficiency. The range of injection timings studied produced changes of 50% and 34% in the CO and HC emissions, respectively. A reduction in NO_x emissions of 35% to 43% was observed for a 3° retarded injection timing compared with a 3° advanced injection timing. A common linear relationship was found between the start of injection and the NO_x emissions for all the fuels studied. When compared at the same start of combustion, the neat biodiesel produced lower NO_x emissions than the No. 2 diesel fuel.

Keywords. *Biodiesel, Diesel, Emissions, Engines, Fuel, Soybean oil.*

Diesel engines are widely used as power sources for medium- and heavy-duty applications because of their lower fuel consumption and lower emissions of carbon monoxide (CO) and unburned hydrocarbons (HC) compared with gasoline engines. For many years, the ready availability of inexpensive middle-distillate petroleum fuels provided little incentive for experimenting with alternative, renewable fuels for diesel engines. However, since the oil crisis of the 1970s, research interest has expanded in the area of alternative fuels. In recent years, the potential environmental benefits of alternative fuels have also attracted attention.

Many researchers have concluded that vegetable oils hold promise as alternative fuels for diesel engines (Goering et al., 1982; Sims, 1985). Using raw vegetable oils in diesel engines can cause numerous engine-related problems. The increased viscosity and low volatility of vegetable oils lead to severe engine deposits, injector coking, and piston ring sticking (Perkins et al., 1991; Pestes and Stanislaw, 1984). However, these effects can be reduced or eliminated through transesterification of the vegetable oil to form a monoester, generally known as "biodiesel" (Perkins et al., 1991; Zhang et al., 1988). This process decreases the viscosity, maintains the heating value, and may actually increase the cetane

number. It has also been found that biodiesel can provide a substantial reduction in HC, CO, and particulate emissions, although often at the cost of an increase in NO_x emissions (Chang et al., 1996; Last et al., 1995; Schumacher et al., 1993).

A number of diesel emissions studies have been conducted with biodiesel and blends of biodiesel, but few have dealt with injection timing effects, and none have included the effects of fuel oxidation on engine emissions and biodiesel combustion. The objective of this study was to evaluate the effect of injection timing and fuel oxidation on biodiesel combustion and exhaust emissions.

EQUIPMENT AND PROCEDURES

ENGINE TEST SETUP AND EXHAUST SAMPLING PROCEDURE

A John Deere 4276T four-cylinder, four-stroke, turbocharged DI diesel engine with a bore of 106.5 mm, a stroke of 127.0 mm, a displacement of 4.53 L, and a compression ratio of 16.8:1 was connected to a 112 kW (150 hp) General Electric model TLC2544 DC electric dynamometer. A portion of the exhaust gas was passed through a 190°C heated sampling line and filter to the emission analyzers. A Beckman model 402 heated flame ionization detector hydrocarbon analyzer and a Beckman model 7003 polarigraphic oxygen monitor were used to measure the concentrations of HC and oxygen (O₂) in the exhaust gas. Two Beckman model 864 infrared analyzers measured the concentrations of CO and carbon dioxide (CO₂) in the engine exhaust. A Thermo Environmental Instruments Inc. Model 42H chemiluminescent NO-NO₂-NO_x analyzer and a Thermo Environmental Instruments Inc. Model 350 chemiluminescent NO-NO₂-NO_x analyzer were used to gather duplicate measurements of the concentration of NO_x.

Article was submitted for review in January 2000; approved for publication by the Power & Machinery Division of ASAE in August 2000.

The authors are **Abdul Monyem**, Design Engineer, Caterpillar, Inc., Mossville, Illinois; **Jon H. Van Gerpen**, *ASAE Member Engineer*, Professor, and **Mustafa Canakci**, Research Assistant, Department of Mechanical Engineering, Iowa State University, Ames, Iowa. **Corresponding author:** Jon H. Van Gerpen, Dept. of Mechanical Engineering, Iowa State University, Ames, IA 50011; phone: 515-294-5563; fax: 515-294-3261; e-mail: jvg@iastate.edu.

A Bosch smoke meter was used to measure the smoke level. The gaseous emissions were expressed on a brake-specific basis and each data point was the average of three independent measurements. An electronic scale and a stopwatch were used to measure the fuel flow rate.

A Kistler model 6061B pressure transducer was installed in the No. 1 cylinder, and a Kistler model 6230M1 pressure transducer was installed in the No. 1 cylinder fuel injection line. The cylinder and injection pressure data were collected using the Labview computer program with a 486 computer and a National Instruments Model ATMIO-16 data acquisition system. The data acquisition system collected the pressure data every 0.25 degrees of crankshaft rotation, and 50 cycles were averaged.

FUEL PREPARATION

The biodiesel was soybean oil-based and was purchased from NOPEC Corporation (Lakeland, Florida). Its chemical properties are given in table 1. The oxidized biodiesel was prepared by heating 83 L of biodiesel to 60°C in a 208-L container while bubbling oxygen (99.6% purity) through the fuel at the rate of 0.4 m³/h. The fuel's peroxide value, as measured by the American Oil Chemist's Society method Cd 8-53 (AOCS, 1993), was used as the indicator of the extent of oxidation. It was desired to elevate the fuel peroxide value quickly without allowing the fuel viscosity to increase excessively. The biodiesel was oxidized from a starting peroxide value of 30-40 meq O₂/kg to 340 meq O₂/kg in 6-8 h. The oxidized and unoxidized biodiesels, their 20% blends (by weight), and the base fuel (No. 2 diesel) were tested in the engine at two different loads (100% and 20%) and at three injection timings (3° advanced, standard, and 3° retarded). The tests were performed at steady-state conditions at a single engine speed of 1400 rpm. The full-load (100%) torque was 258 N-m and the 20% load torque was 52 N-m.

Table 1. Fuel analysis.

	No. 2 Diesel	Biodiesel	Oxidized Biodiesel
Molecular wt.	198	291.6	N.A.
Carbon (%)	86.23	76.14	76.06
Hydrogen (%)	13.14	11.75	11.51
Sulfur (%)	0.034	<0.005	0.010
CetaneNumber (D613)	47.4	51.1	72.7
Heat of Combustion			
Gross (kJ/kg)	45504	39766	38896
Net (kJ/kg)	42716	37273	36454
Hydrocarbon types			
Saturates (%)	64.1	N.A.	N.A.
Olefins (%)	4.9	N.A.	N.A.
Aromatics (%)	31.0	0	0
Viscosity (cS)		4.63	
Free glycerin		0.004	
Monoglycerides (%)		0.352	
Diglycerides (%)		0.132	
Triglycerides (%)		0.152	
Total glycerin (%)		0.131	
Biodiesel Fatty Acid Composition			
Palmitic (16:0) (%)		10.76	
Stearic (18:0) (%)		4.37	
Oleic (18:1) (%)		24.13	
Linoleic (18:2) (%)		51.83	
Linolenic (18:3) (%)		6.81	

N.A. = Not available

DATA ANALYSIS

STATISTICAL ANALYSIS

In addition to the engine operating variables of load, timing, and fuel type, the oxidized fuel batch number and the age of the fuel were included as test variables to determine whether they had any effect on engine emissions. A simple factorial design was not considered to be appropriate for this test because all of the variables could not be tested independently on any given day. Due to the time required to set the fuel injection timing, only a single value could be tested each day. This limitation mandated the use of a split-plot experimental design.

The split-plot statistical design consists of two stages. The first stage is related to the whole plot, and the second stage is related to a subplot. In this design, a single test day is considered a whole plot, and each of the ten test conditions within a day is considered a sub-plot. This split-plot design is shown in tables 2 and 3. The whole plot is a 3×3 Latin square, and within each whole day plot is a 2×5 factorial experiment. A 3×3 Latin square contains 3 rows and 3 columns (table 2). The three treatments (injection timings) are randomly assigned to experimental units within the rows and columns so that each treatment appears in every row and in every column. The 2×5 factorial experiment identifies the ten randomly chosen combinations of load and fuel type to be run each day (table 3). An SAS program was used to analyze the collected data. More extensive explanation of these topics is provided in Ott (1993) and Neter et al. (1996).

CALCULATION OF IGNITION DELAY

Ignition delay was defined as the time between the start of fuel injection and the start of combustion. The start of injection is usually taken as the time when the injector needle lifts off its seat. Because a needle lift detector was not available, the start of injection was defined to be the point when the injection line pressure reached 207 bar, the nozzle-opening-pressure for the injector. The start of combustion was defined in terms of the change in slope of the heat-release rate that occurs at ignition. The heat release rate was calculated using a technique similar to that described by Krieger and Borman (1966).

Table 2. Whole plot (3×3 Latin square).

Batch	Age		
	1	2	3
1	Standard (Day 1)	3° Advanced (Day 2)	3° Retarded (Day 3)
2	3° Retarded (Day 4)	Standard (Day 5)	3° Advanced (Day 6)
3	3° Advanced (Day 7)	3° Retarded (Day 8)	Standard (Day 9)

Table 3. Randomly assigned subplot within each whole plot (2×5 factorial experiment).

Load	Fuel				
	100% HPVB	100% LPVB	20% HPVB	20% LPVB	No. 2 Diesel
100%	10th	5th	9th	3rd	1st
20%	4th	8th	7th	6th	2nd

RESULTS AND DISCUSSION

THE EFFECT OF TIMING ON DIESEL ENGINE EXHAUST EMISSIONS

Figure 1 shows the percent change in emissions compared to the base diesel fuel for the 3° advanced, standard, and 3° retarded injection timings at the full-load engine condition. In these figures, all emissions comparisons are shown relative to the No. 2 diesel fuel at the same timing. A reduction in the CO, HC, and smoke number (SN) were observed for all fuel blends at all injection timings compared with No. 2 diesel fuel. The maximum reduction in these emissions was found for the oxidized biodiesel. However, the NO_x emissions increased for all fuel blends at all injection timings. The smoke number, CO, and HC were decreased by 8% to 63%, 2% to 29%, and 3% to 60%, respectively, while the NO_x emissions increased by 0.5% to 18%. Regardless of the injection timing, the oxidized neat biodiesel reduced the CO and HC emissions by 4% to 15% and 9% to 16%, respectively, compared with unoxidized neat biodiesel. The emissions of CO₂ showed mixed results with the percentage changes being very small.

Figure 2 shows the percent change in emissions at the light-load engine condition for the three timings. At light load, the smoke level was near the detection threshold of the smoke meter, so these measurements were not shown on the figure. As was observed at high load, there was a reduction in CO and HC emissions regardless of the injection timing and fuel. These CO and HC reductions were in the range of 10% to 56% and 6% to 66%, respectively. The oxidized neat biodiesel reduced the CO and HC emissions more than the unoxidized biodiesel by 16% to 25% and 20% to 29%, respectively, over the range of injection timings studied. An increase in NO_x emissions was found for the 3° advanced injection timing, and a reduction in NO_x emissions was found for the 3° retarded injection timing for all fuel blends.

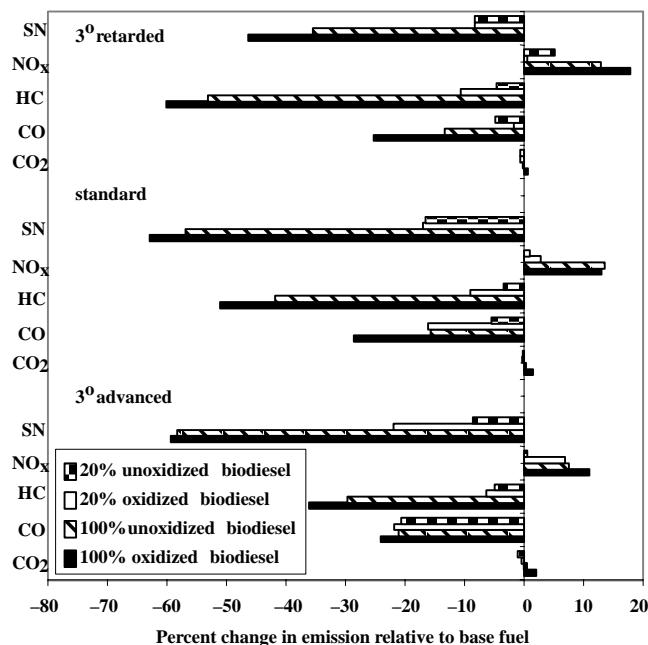


Figure 1. Percent change in emissions relative to base fuel at full-load engine condition.

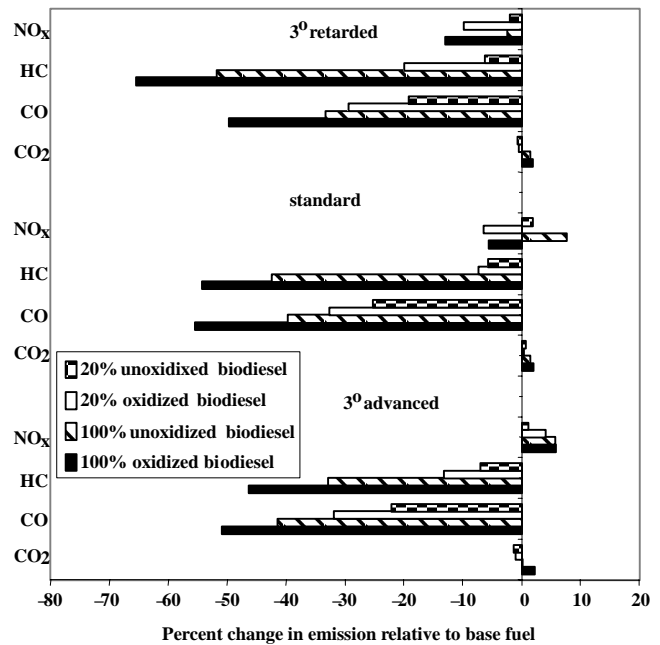


Figure 2. Percent change in emissions relative to base fuel at light-load engine condition.

COMBUSTION CHARACTERISTICS

COMPARISON OF THE START OF FUEL INJECTION

Three different fuel injection pump timing settings were used for this study: 3° retarded, standard, and 3° advanced. The degrees of timing change refer to crankshaft degrees. The actual start of fuel injection is affected by the pump setting, but it can also be influenced by changes in fuel properties such as the viscosity, the bulk modulus, and the speed of sound (Obert, 1973). The start of fuel injection is important because fuel injected early produces higher flame temperatures and may contribute to higher NO_x emissions.

The effect of changes in fuel injection timing on the start of combustion is complicated by the effect of the different fuel cetane numbers. The cetane number is an indicator of the time delay between when the fuel is injected and when it starts to burn.

The injection line pressure with standard timing and at the full-load engine condition for all five tested fuels is shown in figure 3. Even though the fuel injection pump timing was

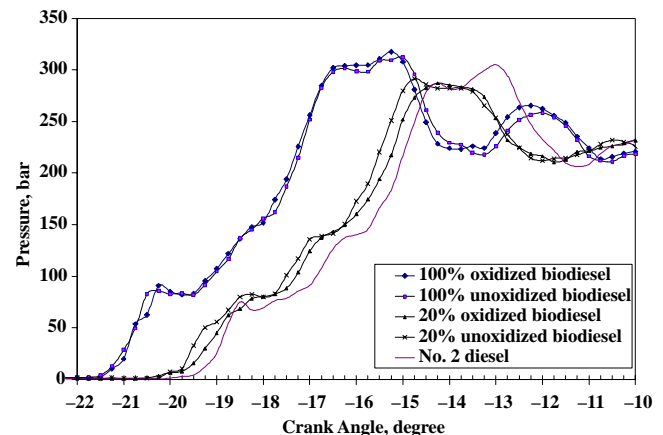


Figure 3. Injection line pressure with standard timing and full-load engine condition.

not altered as the fuels were changed, it is clear that the neat biodiesel fuels had earlier actual injection timings. The oxidized and unoxidized biodiesel fuels both injected about 2.3° earlier than the No. 2 diesel fuel. The 20% blends were $0.25\text{--}0.75^\circ$ earlier than the No. 2 diesel fuel.

Figure 4 shows the start of fuel injection into the cylinder for all three injection timings (3° advanced, standard, and 3° retarded) at the full-load engine condition. Each bar on these figures is the average of three measurements collected on separate days. The error bands show the extent of the maximum and minimum values of the three measurements. The injection timings were set every day and were confirmed using the data acquisition system. Figure 4 shows a consistent tendency for earlier injection timing by the neat biodiesel fuels due to differences in their physical properties.

COMPARISON OF THE START OF COMBUSTION TIMES AND FUEL BURNING RATES

In this study, start of combustion was defined as the time when the heat-release rate calculated from the cylinder pressure data started to rise rapidly. Figure 5 shows the heat-release profiles with standard timing for all five fuels. The oxidized biodiesel showed the most advanced start of combustion. This was expected based on its high cetane number, as reported in table 1. The next most advanced start

of combustion was found for the unoxidized biodiesel. The 20% blends and No. 2 diesel fuel show almost no difference in the start of combustion. Compared to the base fuel, the oxidized biodiesel had about 3.3° earlier start of combustion with standard timing, while the unoxidized biodiesel had only 2.3° earlier start of combustion.

Figures 6 and 7 show the measured start of combustion with the three different timings at the full-load (fig.6) and light-load (fig 7) engine conditions. The start of combustion was earlier for the oxidized biodiesel compared to No. 2 diesel fuel. The unoxidized biodiesel also advanced the start of combustion, but the other fuels (the 20% blends and No. 2 diesel) showed somewhat mixed results at the full-load engine condition. At the light-load engine condition, the start of combustion was more retarded than at the full-load engine condition. The oxidized biodiesel at this load showed the most advanced start of combustion, while the No. 2 diesel fuel showed the most retarded. These differences in the start of combustion are the result of two factors: 1) Biodiesel should have a shorter ignition delay, as indicated by its higher cetane number, and 2) Biodiesel's different physical properties, such as higher bulk modulus, viscosity, and speed of sound, can also cause an earlier injection event (Gouw and Vlughter, 1964; Tat and Van Gerpen, 1999; Tat et al., 2000).

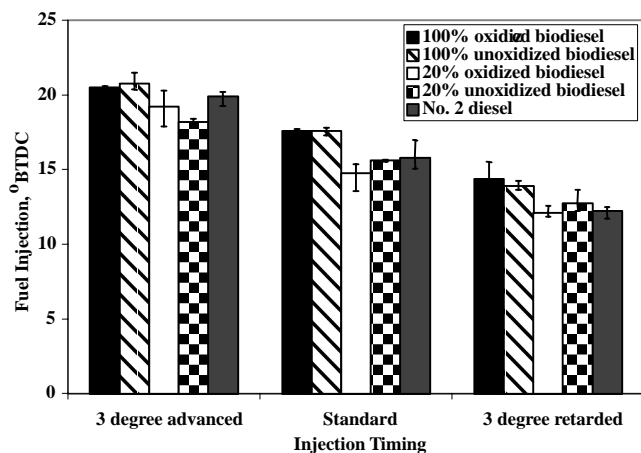


Figure 4. Fuel injection at full-load engine condition.

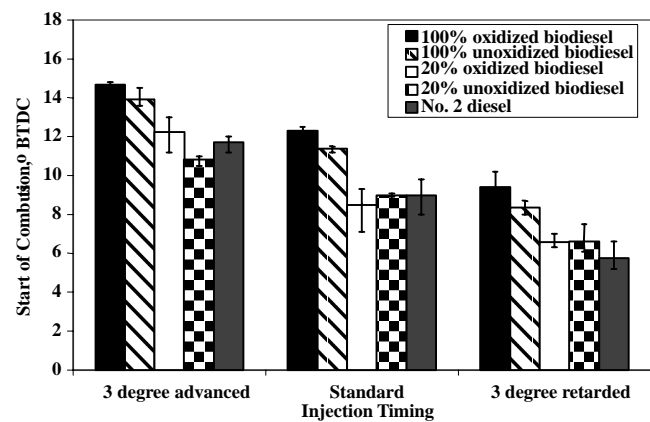


Figure 6. Start of combustion at full-load engine condition.

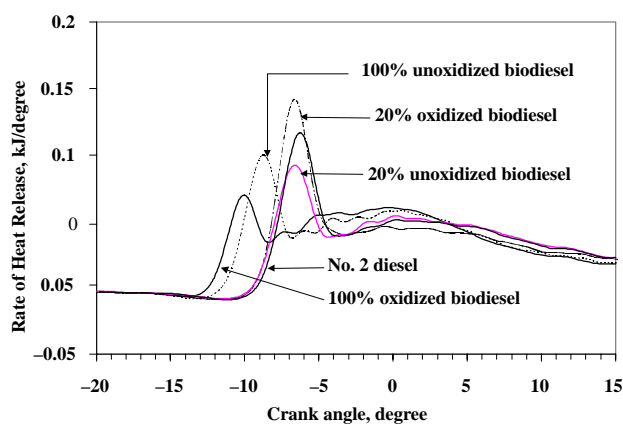


Figure 5. Heat-release profiles with timing at full-load engine condition.

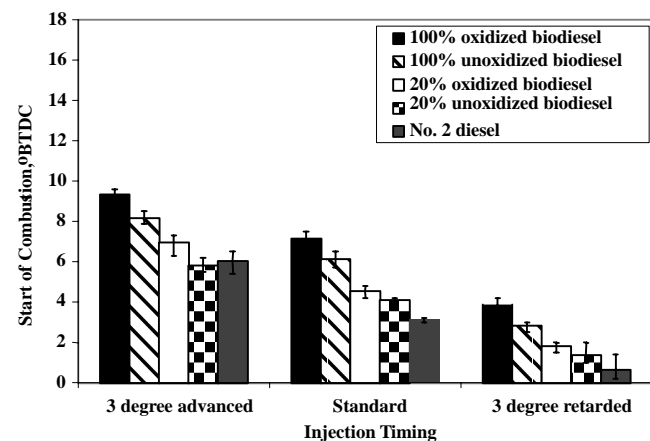


Figure 7. Start of combustion at light-load engine condition.

DISCUSSION OF OBSERVED TRENDS

EFFECT OF IGNITION DELAY ON HC EMISSIONS

Most HC emissions in diesel engines originate in regions where excessive dilution with air prevents combustion because the fuel–air mixture is past the lean combustion limit. The magnitude of the unburned HC from these over–lean regions is related to the amount of fuel injected during the ignition delay period, before combustion starts. Figure 8 confirms this correlation between HC emissions and ignition delay for the light–load operating condition, where the HC emissions are highest. This figure includes data for all five fuels and all three injection timings. The data show the expected trend: the HC emissions decrease as the ignition delay gets shorter. The HC emissions for all fuels and for all injection timings appear to fall on one line. This correlation was unexpected given the large differences in volatility and oxygen content of these fuels.

EFFECT OF THE START OF FUEL INJECTION AND THE START OF COMBUSTION ON NO_x EMISSIONS

Generally, NO_x emissions form in the high–temperature regions of the combustion chamber, where the air/fuel ratio is slightly below stoichiometric. Springer and Patterson (1972) noted that increases in the local temperature and the oxygen concentration within the diesel spray envelope increase the NO_x emissions. One theory that has been proposed for the increased NO_x observed with biodiesel is that the oxygen contained in the fuel makes more oxygen available in the reaction zone during combustion, and this causes the NO_x emissions to rise (Rickeard and Thompson, 1993).

To investigate the effect of biodiesel combustion on the flame temperature, calculations were performed to determine the adiabatic flame temperature for biodiesel combustion compared with diesel fuel combustion. Figure 9 shows the stoichiometric adiabatic flame temperature for biodiesel and for No. 2 diesel fuel. The calculations show that for both constant–volume combustion and constant–pressure combustion, the flame temperature for biodiesel is slightly below that for diesel fuel. This indicates that flame temperature changes alone cannot adequately explain the higher levels of NO_x observed with biodiesel.

The emissions comparisons presented in this article were conducted with the engine adjusted to produce the same torque level with each fuel. This means that the fuel flow rate of the biodiesel was increased compared with diesel fuel to compensate for biodiesel’s lower energy content. Because most engines are limited by the volume of fuel that can be injected, many researchers have evaluated biodiesel in unmodified engines, where biodiesel’s lower energy content causes lower maximum torque. Figure 10 shows a comparison of the adiabatic flame temperature for diesel fuel at an equivalence ratio of 0.6, a typical full–load value, with the flame temperature for biodiesel at 0.5434, a value that corresponds to the same volume of fuel delivery. In this case, the flame temperatures are substantially lower for biodiesel. These data further indicate that flame temperature is probably not the reason for the higher NO_x levels observed with biodiesel.

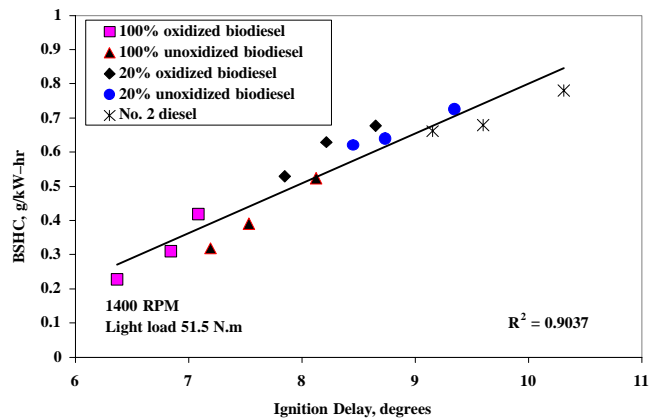


Figure 8. Brake–specific HC emissions as a function of ignition delay at light–load engine condition.

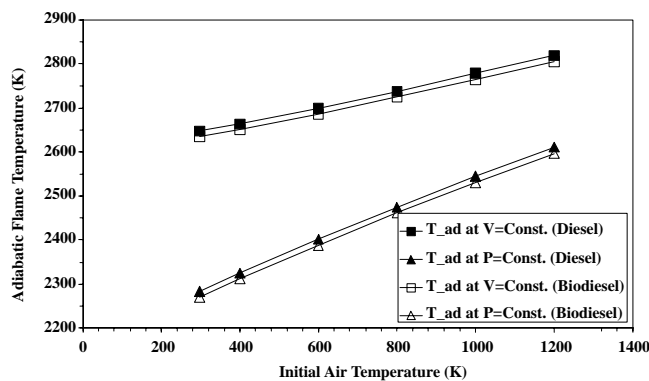


Figure 9. Stoichiometric adiabatic flame temperature for biodiesel and diesel fuel.

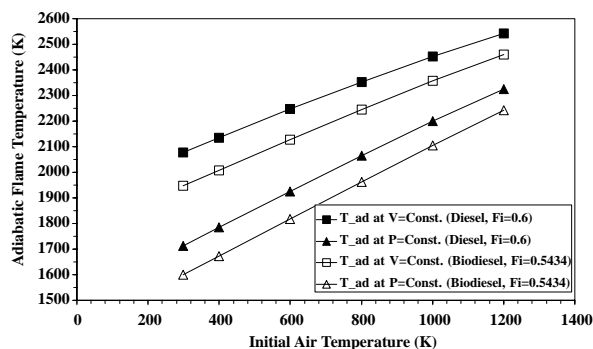


Figure 10. Adiabatic flame temperature for equal fuel volumes of biodiesel and diesel fuel.

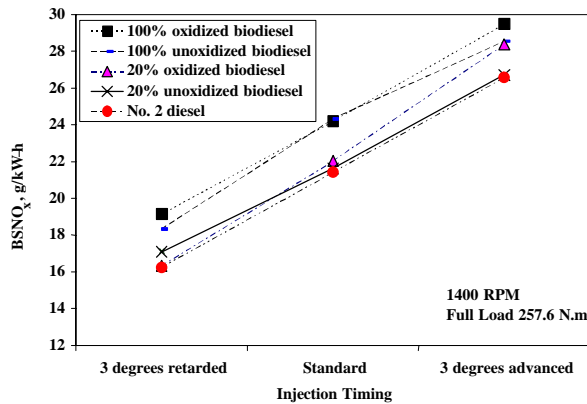


Figure 11. Brake-specific NO_x emissions vs. pump timing at full-load engine condition.

The NO_x emissions with the three different pump timings at the full-load engine condition are shown in figure 11. It is clear from this figure that both the injection timing at the pump and the fuel type have a strong effect on NO_x emissions. As observed by other researchers (Rickeard and Thompson, 1993; Scholl and Sorenson, 1993; Ali, 1995; Feldman and Peterson, 1992; Mittelbach and Trillhart, 1988), the NO_x emissions increase as the injection timing is advanced, and the NO_x emissions for 100% biodiesel are higher than for diesel fuel or the 20% blends.

The pump timings shown in figure 11 are nominal values, not the actual fuel injection timing. Because biodiesel has a different viscosity, bulk modulus, and speed of sound than diesel fuel, the actual fuel injection timing for biodiesel was different than for diesel fuel, even at the same nominal pump timing. Biodiesel is less compressible than diesel fuel, so pressure can develop faster—and pressure waves can propagate faster—in biodiesel than in diesel fuel. This is the reason for the advanced injection timing of biodiesel noted earlier. This advanced injection may contribute to the additional NO_x emissions for biodiesel. To investigate this effect, the full-load NO_x emissions were plotted against the actual injection timing, as shown in figure 12. The NO_x emissions for all fuels and all pump timings appear to fall on one line when plotted against the actual start of injection. This indicates that the difference in NO_x emissions can be explained by variations in the true start of fuel injection and may not be fuel-dependent.

Although fuel injection timing appears to correlate to the measured NO_x emission levels, the start of combustion would be a more direct parameter to use for correlating NO_x because combustion is the process that produces NO_x. This correlation would also incorporate differences in the ignition delay periods between biodiesel and diesel fuel that are based on differences in the cetane number. Figures 5, 6, and 7 showed that the start of combustion was more advanced for biodiesel than for diesel fuel due to its higher cetane number, causing a shorter ignition delay and conforming to biodiesel's earlier actual injection timing. However, the shorter ignition delay will also cause less premixed combustion, which has been identified as a source of NO_x

production in naturally aspirated and lightly turbocharged engines (Chan and Borman, 1982).

When the NO_x data are plotted against the start of combustion, as shown in figure 13, differences between the fuels emerge again. These plots indicate that for the same start of combustion timing, the 100% biodiesel fuels actually produced less NO_x than diesel fuel. This result is probably attributable to the lower amount of premixed combustion with biodiesel due to its higher cetane number. This result may be engine-specific because Donahue, et al. (1994) have noted that the correlation between premixed combustion and NO_x decreases for highly turbocharged engines.

TRADEOFF BETWEEN NO_x EMISSIONS AND SMOKE EMISSIONS

Figure 14 shows the tradeoff relationships between the NO_x emissions and the smoke number as the actual fuel injection timing was varied. The figure indicates that, for this diesel engine, oxidized neat biodiesel shows a better tradeoff than No. 2 diesel fuel. The tradeoff curves for neat unoxidized biodiesel and the 20% blends are between oxidized neat biodiesel and No. 2 diesel fuel.

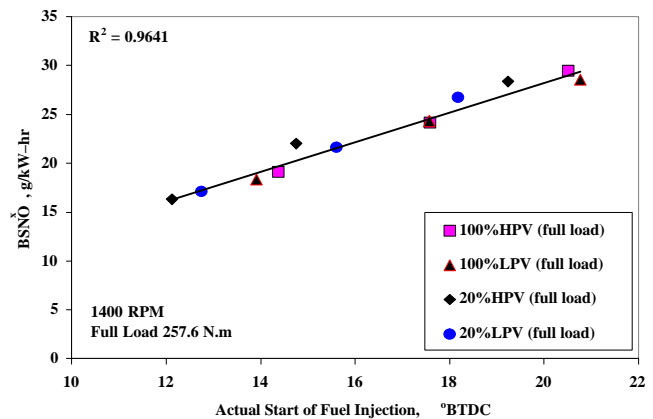


Figure 12. Brake-specific NO_x emissions as a function of start of fuel injection.

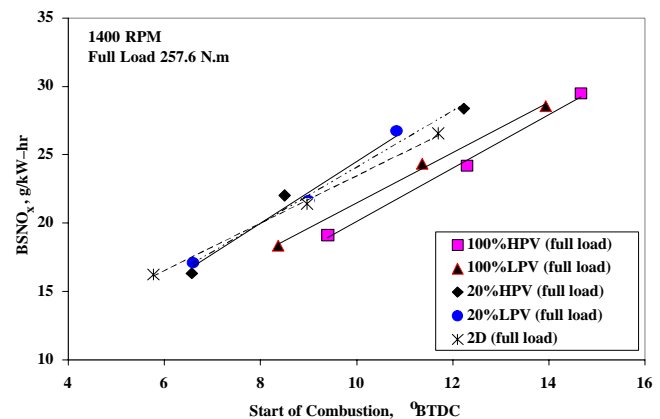


Figure 13. Brake-specific NO_x emissions as a function of start of combustion at full-load engine condition.

CONCLUSIONS

The objectives of this study were to understand the effect of timing and fuel oxidation on biodiesel exhaust emissions and combustion. Based on the experimental results and the above discussion, the following conclusions can be drawn:

1. Biodiesel, particularly if oxidized, has lower CO and HC emissions than No. 2 diesel fuel. The retarded injection timing produced 50% less CO emissions and 34% less HC emissions than the advanced injection timing for neat oxidized biodiesel.
2. Retarded injection timing significantly reduced NO_x emissions. The 3° retarded injection timing gave a 20.9% reduction in NO_x emissions for neat oxidized biodiesel at the full-load engine condition compared with standard injection timing.
3. Injection timing had a significant effect on smoke number. The advanced injection timing gave a lower smoke number than the retarded injection timing. The Bosch Smoke Number for the oxidized biodiesels increased from 0.4 (for the 3° advanced timing) to 1.0 (for the 3° retarded timing). The Bosch Smoke Number for No. 2 diesel fuel increased from 1.0 to 1.9 over this range of timings.
4. The actual fuel injection timing was advanced for neat biodiesel compared with diesel fuel at the same injection pump settings due to differences in the physical properties of the fuels. Compared with diesel fuel, the fuel injection timing for the two neat biodiesels was about 2.3° advanced.
5. The oxidized and unoxidized biodiesels experienced shorter ignition delays than diesel fuel and had less pre-mixed burning. The neat oxidized biodiesel had a 0.9° shorter ignition delay than the neat unoxidized biodiesel at standard timing. Retarded injection timing reduced the ignition delay for all fuels.
6. Shorter ignition delay reduced HC emissions. The ignition delay was linearly correlated to HC emissions with no effect of fuel type.
7. A common linear relationship was found between NO_x emissions and the start of fuel injection that showed no effect of fuel type. However, when NO_x was plotted against the start of combustion, there were differences between the fuels. At the same start of combustion, the neat biodiesel fuels were found to produce less NO_x than the No. 2 diesel fuel.
8. The relationship between NO_x emissions and smoke number for biodiesel showed that both oxidized and unoxidized biodiesels provide a superior tradeoff compared with No. 2 diesel fuel.

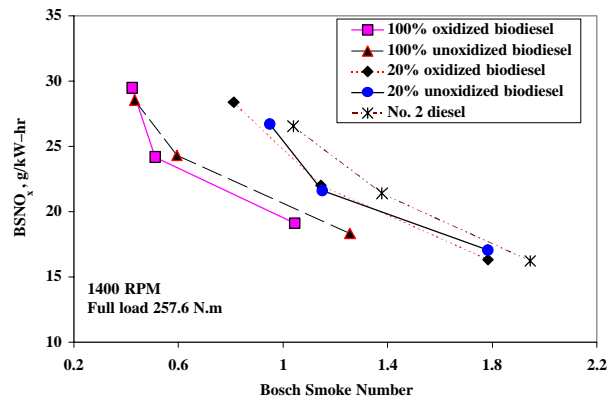


Figure 14. Brake-specific NO_x vs. smoke number at full-load engine condition.

REFERENCES

- Ali, Y. 1995. Beef tallow as a biodiesel fuel. Ph.D. diss. University of Nebraska, Lincoln.
- AOCS. 1993. 4th Ed. *Official Methods and Recommended Practices of the American Oil Chemists' Society*. Champaign, Ill.: AOCS Press.
- Chan, T. T., and G. L. Borman. 1982. An experimental study of swirl and EGR effects on diesel combustion by use of the dumping method. SAE Paper No. 820359. Warrendale, Pa.: SAE.
- Chang, D. Y. Z., J. H. Van Gerpen, I. Lee, L. A. Johnson, E. G. Hammond, and S. J. Marley. 1996. Fuel properties and emissions of soybean oil esters as diesel fuel. *JAOCs* 73(11): 1549–1555.
- Donahue, R. J., G. L. Borman, and G. R. Bower. 1994. Cylinder-averaged histories of nitrogen oxide in a D.I. diesel with simulated turbocharging. SAE Paper No. 942046. Warrendale, Pa.: SAE.
- Feldman, M. E., and C. L. Peterson. 1992. Fuel injection timing and pressure optimization on a DI diesel engine for operation on biodiesel. *Liquid Fuels From Renewable Resources: Proceedings Of An Alternative Energy Conference*, 14–15 December. St. Joseph, Mich.: ASAE.
- Goering, C. E., A. W. Schwab, M. J. Dangherty, E. H. Pryde, and A. J. Heakin. 1982. Fuel properties of eleven vegetable oils. *Trans. ASAE* 25(6): 1472–1477, 1483.
- Gouw, T. H., and J. C. Vlugter. 1964. Physical properties of fatty acid methyl esters, IV. Ultrasonic sound velocity. *JAOCs* 41(8): 524–526.
- Krieger, R. B., and G. L. Borman. 1966. The computation of applied heat release for internal combustion engines. ASME Paper No. 66-WA/DGP-4. New York, N. Y.: ASME.
- Last, J. R., M. K. Kruger, and M. Durnholz. 1995. Emissions and performance characteristics of a 4-stroke, direct injection diesel engine fueled with blends of biodiesel and low sulfur diesel fuel. SAE Paper No. 950054. Warrendale, Pa.: SAE.
- Mittelbach, M., and P. Trillhart. 1988. Diesel fuel derived from vegetable oils, III. Emission tests using methyl esters of used frying oil. *JAOCs* 65(7): 1185–1187.

- Neter, J., M. H. Kutner, C. J. Nachtsheim, and W. Wasserman. 1996. *Applied Linear Statistical Models*. Chicago, Ill.: McGraw-Hill.
- Obert, E. F. 1973. *Internal Combustion Engines and Air Pollution*. New York, N. Y.: Intext.
- Ott, L. R. 1993. *An Introduction to Statistical Methods and Data Analysis*. Belmont, Calif.: Marion Merrell Dow, Inc.
- Perkins, L. A., C. L. Peterson, and D. L. Auld. 1991. Durability testing of transesterified winter rape oil (*Brassica Napus* L.) as fuel in small bore, multi-cylinder, DI, CI engines. SAE Paper No. 911764. Warrendale, Pa.: SAE.
- Pestes, N. M., and J. Stanislaw. 1984. Piston ring deposits when using vegetable oil as a fuel. *Journal of Testing and Evaluation* 12(2): 61–68.
- Rickeard, D. J., and N. D. Thompson. 1993. A review of the potential for bio-fuels as transportation fuels. SAE Paper No. 932778. Warrendale, Pa.: SAE.
- Scholl, K. W., and S. C. Sorenson. 1993. Combustion of soybean oil methyl ester in a direct injection diesel engine. SAE Paper No. 930934. Warrendale, Pa.: SAE.
- Schumacher, L. G., S. C. Borgelt, W. G. Hires, C. Spurling, J. K. Humphrey, and J. Fink. 1993. Fueling diesel engines with esterified soybean oil. ASAE Paper No. MC93–101. Presented at the 1993 Mid-Central Conference of the ASAE. St. Joseph, Mich.: ASAE.
- Sims, R. E. H. 1985. Tallow esters as an alternative diesel fuel. *Trans. of the ASAE* 28(3): 716–721.
- Springer, G. S., and D. J. Patterson. 1972. *Engine Emissions: Pollutant Formation and Measurement*. New York, N. Y.: Plenum Press.
- Tat, M. E., and J. H. Van Gerpen. 1999. The kinematic viscosity of biodiesel and its blends with diesel fuel. *JAOCS* 76(12): 1511–1513.
- Tat, M. E., J. H. Van Gerpen, S. Soylu, M. Canakci, A. Monyem, and S. Wormley. 2000. The speed of sound and isentropic bulk modulus of biodiesel at 21°C from atmospheric pressure to 35 MPa. *JAOCS* 77(3): 285–289.
- Zhang, Q., M. Feldman, and C. L. Peterson. 1988. Diesel engine durability when fueled with methyl ester of winter rapeseed oil. ASAE Paper No. 88–1562. St. Joseph, Mich.: ASAE.